Journal of Sol-Gel Science and Technology (2022) 103:1–11
https://doi.org/10.1007/s10971-022-05805-0

REVIEW PAPER: FUNDAMENTALS OF SOL-GEL AND HYBRID MATERIALS PROCESSING

Impact of bismuth titanate for microwave absorber application: a review

P. Harshapriya[1] · Deepak Basandrai[1]

Received: 10 November 2021 / Accepted: 4 April 2022 / Published online: 27 April 2022

Abstract

Bismuth titanate (BTO) owe to high dielectric constant, high dielectric losses, and high temperature coefficient of resonant frequency is considered to be one of the most prominent aspirants for microwave absorption applications. BTO and their composites are also used to diminish the electromagnetic interference in electrical devices, Airplanes, ships and tank radar signals. Several studies have been reported to enhanced the capability of BTO for microwave absorption applications. In such studies, the ferroelectric and dielectric characteristics of $Bi_4Ti_3O_{12}$ are found to be improved by doping it with V, La, Sm, and Nd as compared to other dopants. However, Sm-Ta co doped BTO has shown high remanent polarization (46.2 emu/g) and coercive field (102 Oe). The highest dielectric loss was observed in vanadium doped $Bi_4Ti_3O_{12}$ which enable it for high temperature applications.

Graphical abstract

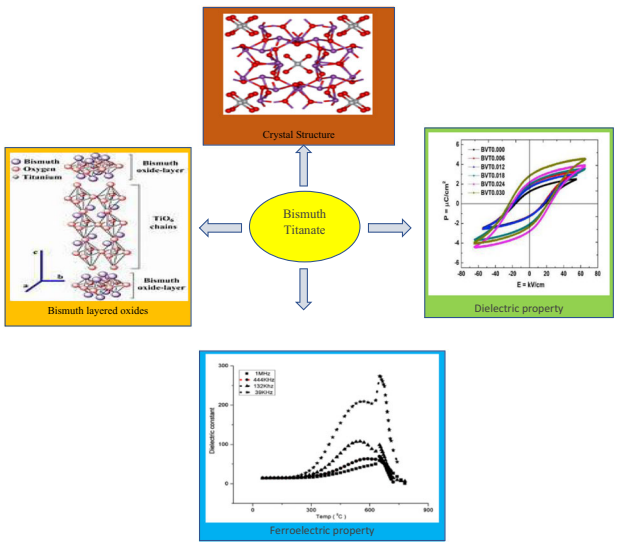

Keywords Microwave absorption · Dielectric property · Ferroelectric property · Bismuth titanate · Structural properties

1 Introduction

Microwave is a type of electromagnetic radiation with frequencies going from around 1 m to 1 mm comparing to frequencies between 300 MHz and 300 GHz separately. They obey the principles of optics and, depending on the

✉ Deepak Basandrai
deepak.basandrai@lpu.co.in

[1] Department of Physics, School of Physical Sciences and Chemical Engineering, Lovely Professional University, Phagwara, Punjab 144411, India

type of substance, can be transmitted, absorbed, or reflected. Microwave absorbs with the best thermal stability, antioxidant capability, low density, a broad absorption frequency range, and strong absorption qualities are typically required [1]. Different magnetic ferrite compounds have recently emerged as a promising candidate for microwave absorption applications. These materials have been intensively explored due to their incredible magnetic loss capabilities; however, their applications are limited due to clean agglomeration and excessive density [2]. Both electric and magnetic dipoles should have powerful microwave absorbers for microwave absorption. Furthermore, compositing's dielectric-magnetic characteristics are a potent method for improving microwave attenuation. Barium titanate, bismuth titanate, barium ferrite, $BiFeO_3$, $BiVO_4$, and other barium and bismuth-based microwave absorption materials have recently received a lot of interest. Bismuth titanate layered-structured ferroelectrics are appealing from the point of view of their application as electronic materials such as dielectrics, piezoelectric, and pyroelectrics, because they have good piezoelectric properties stability, a high Curie temperature, and a good resistance vs temperature [3].

Lead-free ceramics have been broadly utilized as ferroelectric materials as they are less toxic and are environmentally friendly [4]. The bismuth titanium oxide ($Bi_4Ti_3O_{12}$) is a lead-free compound of the Aurivillius stage with alternating oxide $(Bi_2O_2)^{2+}$ and perovskite-like $(Bi_4Ti_3O_{10})^{2-}$layers along the *c* axis. Bismuth titanate is a well-known member of bismuth layer-structured ferroelectrics. It has a strong anisotropic property. Bismuth titanate is large quickly accessible in most volumes. High purity, submicron and nano powder structures might be considered. Bismuth titanate is important from a scientific and technological point of view because, it exhibits ferroelectric properties up to the temperature of 675 °C, which is larger as compared to the lead zirconate titanate (~380 °C) [5]. $Bi_4Ti_3O_{12}$ is a ferroelectric phase with a relatively high dielectric constant of ~200 and high dielectric strength. Titanate compounds comprise a form of titanium oxide and are used in ceramics, electronics, and batteries, among other things (on account of lithium titanate). Bismuth titanates exhibit electrooptical and photorefractive impact, i.e., a reversible change in the refractive list in response to an applied electric field or illumination. Following that, they might be used in reversible recording media for continuous holography or image processing.

The dielectric and ferroelectric characteristics of bismuth titanate, which were synthesized using several methods, are discussed in this article. A high temperature coefficient of resonant frequency, a high dielectric constant, and a high dielectric loss are all required for an ideal microwave absorber. Numerous research groups have discovered these characteristics. As a result, it is better to use bismuth titanate as a microwave absorber. It will definitely be required in the future to compare the characteristics of bismuth titanate in order to determine their applications.

2 Structure

$Bi_4Ti_3O_{12}$ is a multilayer ferroelectric oxide made of bismuth. The chemical formula for bismuth titanate is $Bi_{12}TiO_{20}$, $Bi_4Ti_3O_{12}$, or $Bi_2Ti_2O_7$ [6]. The structure of the Aurivillius stages can be effortlessly clarified utilizing the formula $(Bi_2O_2)^{2+}$ $(M_{n-1}RnO_{3n+1})^{2-}$, where *n* is any number somewhere in the range of 1 and 6. $(M_{n-1}RnO_{3n+1})^{2-}$ recipe is comprised of *n* pseudo perovskite units that are sandwiched between two layers of $(Bi_2O_2)^{2+}$ [7]. The M cation is a major mono, di, or trivalent cation, e.g., Na^+, Bi^{3+}, Pb^{2+}, though the R cation is more modest tri, tetra, penta, or hexavalent cation [8, 9]. An alkali or alkaline earth cation is represented by M. The letter R stands for diamagnetic transition metal [10]. The sequence of Bi_2O_2 and perovskite-like $M_{n-1}RnO_{3n+1}$ layers make up the structure of Aurivillius oxides. Since Aurivillius' original work, a few different compounds with this overall equation have been incorporated and described, including $SrBi_2Ta_2O_9$ ($n = 2$), $Bi_4Ti_3O_{12}$ ($n = 3$), etc. [11–14]. A simplified crystal structure of $Bi_4Ti_3O_{12}$ is displayed in Fig. 1a, b [14]. The bismuth oxide layers and three pseudo perovskite units have been identified. The crystallographic design of $Bi_4Ti_3O_{12}$ ceramic was separated at room temperature by XRD. [15, 16]. The unit cell attributes of $Bi_4Ti_3O_{12}$ were found to be *a*, *b*, *c* as 5.409 Å, 5.449 Å, and 32.816 Å respectively, demonstrating that the structure is orthorhombic [17]. Unit cell parameters of pure and doped $Bi_4Ti_3O_{12}$ were given in Table 1. As the Er content in $Bi_4Ti_3O_{12}$ increases, so does the overall cell volume and averaged particle size. Lead-free bismuth titanate also has an orthorhombic structure with a crystalline size of particle 18.8 nm and the sample contains no impurity peaks and the formation of the agglomerate is large [16]. Fouskova et al. was presented a quantitative clarification of the low-frequency dispersions observed in bismuth titanate crystals. Low-temperature maxima are apparent in pseudo-orthorhombic ϵ_a, ϵ_b, and ϵ_e, however, relaxation character starts from a space-charge which is produced by the inhomogeneity in the exceptionally high conductivity or at the surface of the crystal [18]. Rachna et al. explored lanthanum ion replaced bismuth titanate. The orthorhombic lattice alteration was decreased by La replacement at *x* as 0.75 in Bismuth titanate, however, no phase shift from orthorhombic to tetragonal was observed. With La-doping, the orthorhombic alteration was found to diminish from 9.2×10^{-3} to 1.85×10^{-3} [19]. Thirur-amanathan et al. utilized the combustion process to make bismuth titanate nanopowder for assembling a microstrip

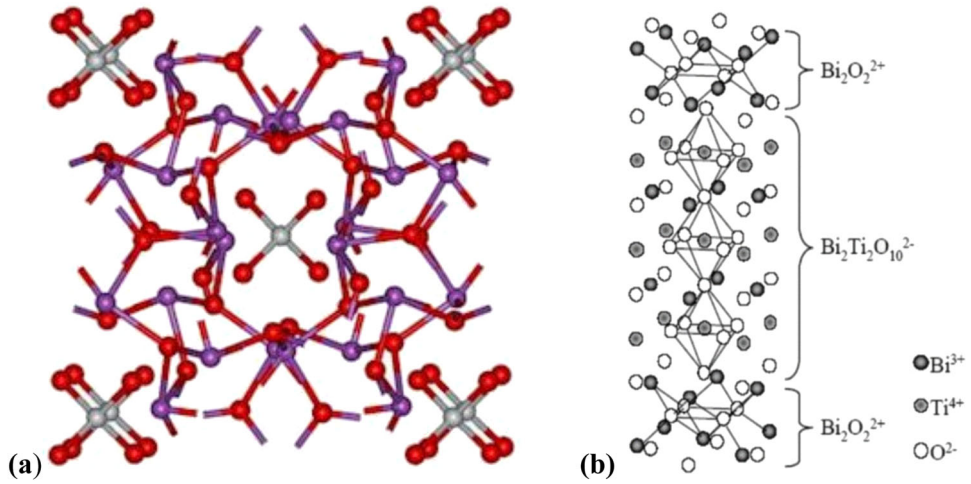

Fig. 1 **a** Crystal Structure of Bismuth Titanate. **b** The bismuth oxide layers and pseudo perovskite units are shown in this idealized structure of $Bi_4Ti_3O_{12}$ [14]

Table 1 Unit cell parameters of doped and undoped $Bi_4Ti_3O_{12}$

Sample	a(Å)	b(Å)	c(Å)	V(Å)^3	Properties	Ref
Er-doped $Bi_4Ti_3O_{12}$	5.429	5.424	32.558	958.73	Enhancement of Up-conversion luminescence property	[33]
V-doped $Bi_4Ti_3O_{12}$	5.4076	5.4438	32.820	966.15	Enhance ferroelectric and dielectric properties.	[21]
Nd-doped $Bi_4Ti_3O_{12}$	5.378	5.381	32.826	949.9	Enhance magnetization, improvement ferroelectric, dielectric properties.	[22]
$Bi_4Ti_3O_{12}$	32.8137	5.4063	5.44135	965.28	Enhance electrical property	[23]
La-doped $Bi_4Ti_3O_{12}$	5.4076	5.4438	32.820	966.15	Enhance ferroelectric, impedance properties, low dielectric constant	[34]

rectangular patch antenna. The selected area electron diffraction pattern confirmed the orthorhombic phase of BTO. The hysteresis curves illustrate that as the electric field gets stronger, so does the coercivity and remanence polarization [20].

On doping vanadium, a limited quantity of vanadium doesn't influence the fundamental BTO orthorhombic design and there is no considerable change in morphology with the vanadium doping sample as it is a plate-like anisotropic structure. The relative density of the samples declines up to 97% for vanadium doped $Bi_4Ti_3O_{12}$. An increment in vanadium doping prompts an increase in density because of the combination of vanadium in $Bi_4Ti_3O_{12}$ ceramic equal to 0.024 mol% and it decreases at 0.03 mol% [21]. On doping rare-earth (La, Sm, Nd) with bismuth titanate, the rare earth cations could substitute completely at the Bi sites in $Bi_4Ti_3O_{12}$ up to $x = 2.5$ at 1100 °C. The lattice parameter for Nd-2.5 is reported that a, b, c as 0.5378 nm, 0.5381 nm, 3.2826 nm respectively. b/a as 1.001, and $V = 0.9499\ nm^3$ based on the orthorhombic system [22]. Yuen et al. presented diffraction peaks of bismuth titanate as a cubic structure with no trace of impurity phase [23].

Xiang et al. make bismuth titanate-based composites along with silver particles. In the composites, no reaction phase between the $Bi_{12}TiO_{20}$ matrix and the silver was observed. With the $Bi_{12}TiO_{20}$ matrix and a microstructure comprising of plate-like grains having an anisotropic form and equiaxed particles, the metallic silver phase is viable. The silver particles are scattered at the grain-boundary region and in the higher BiT plate-like grains [24]. By expanding the reaction temperature or enlarging the reaction period aids crystal formation. The morphology of the samples shifts from spherical to irregular polyhedrons as the reaction time increases. The bandgap of the prepared sample is 2.76 eV [25]. $Bi_{12}TiO_{20}$ nanoparticles have a micro sheet morphology, which means they have excellent sheet images and are in the micrometer range within the face center cubic structure. $Bi_{12}TiO_{20}$ has high efficiency and a 95% methylene blue degradation percentage, as well as strong sensitivity [26]. On doping Nd and Sm, raising the Nd concentration to 1 mol brought about a critical decrease in grain size. The Nd doping trend was similar to the Sm doping trend. Both findings suggest that Nd and Sm have a considerable impact on grain size homogeneity, especially at high mole content (1.0). At the point when the amount of rare-earth was expanded from 0.25 to 1 mol, the dielectric constant of Nd doping raises by 82% and 70%, individually. The rise in ε_r in the Sm doping system, on the other hand, was only about 12% from 0.25 to 1.0 mol. The considerable difference in ε_r between Nd and

Sm, notably at 1.0, can be explained by the relaxation of orthorhombic distortion and octahedral tilting in a multilayer structure [27, 28]. A tendency for 00l-type indices was observed in lanthanum-doped bismuth titanate ceramics. Favored orientation decreased as the concentration of La increased. The drop in preferred grain orientation appears to be linked to the decrease in grain size. $Bi_3La_1Ti_3O_{12}$ ceramic exhibited a broad dielectric peak at T_c 280 °C and a reduction of dielectric maxima, whereas $Bi_{3.25}La_{0.75}Ti_3O_{12}$ ceramic had a sharp peak at T_c 417 °C [29]. Badapanda et al. presented dysprosium doped barium bismuth titanate. The production of substances with no secondary phase signature was observed. The lesser ionic radii of Dy^{3+} associated with Bi^{+3} resulted in a decrease in the lattice parameter [30]. Bi ions were exclusively substituted by Nd ions at the Ti–O octahedron layers in this bi-layered perovskite structure for Nd-doped bismuth titanate. It also has a random orientation and a plate-like form [31, 32].

Bismuth titanate has been prepared by Solid state, conventional mixed oxide method, hydrothermal, combustion route, sol–gel synthesis etc. Fuentes et al. used a combination sol–gel hydrothermal method to prepare Er^{3+}-doped bismuth titanate nanoparticles at a partial oxygen pressure of 30 bar. At room temperature, XRD supports the orthorhombic perovskite structure. As Er concentration rises, cell volume and average particle size decrease (from 32.7 to 21.9 nm). The crystals have spherical, plate-like and agglomerate size bigger than 5 µm [33]. Badge and Deshpande used the sol–gel process to synthesize vanadium doped and lanthanum doped bismuth titanate, which was then calcined at 400 °C for 3 h to examine its structural, dielectric, and ferroelectric characteristics. The addition of a small quantity of *V* has no effect on the basic BTO orthorhombic structure, indicating that the BVT samples are single-phase with particle size 37 nm. The BVT structure is plate-like, comparable to that of BTO ceramics, there is no significant change in morphology with vanadium doping. In nature, the grains are mainly anisotropic and for higher concentration, porosity increases. In case of La- doped BTO, Additional peaks linked with the impurity phases La_2 (Ti_2O_7), $Bi_2Ti_2O_7$, and La_2TiO_5 were identified at modest intensities. This suggests that during the sintering (1000 °C for 3 h) of BLT ceramics, certain changes in crystal structure occurred. These impurity phases in ceramics appear after sintering, which might be attributed to high bismuth volatilization during the sintering process. With an average grain size of 2 µm, a typical plate-like morphology was seen. When bismuth titanate is modified with La^{3+}, the grain size reduces. In larger concentrations of BLT, fine grains appear between large anisotropic grains. It is possible that this is due to impurity stages and the change in microstructure is related to the replacement of Bi^{3+} ions with La^{3+} ions, which are volatile at high temperatures. [21, 34]. Soft combustion was used to make bismuth titanate with varying lanthanum (La) concentrations (0.25, 0.50, 0.75, and 1.0 mol%) sintered 1000 °C for 3 h. In this process the prepared precipitate paste was kept in oven for 80 °C over night for getting it dried and to combust into powder, the dry powder was heated on a hot plate. A thermocouple (K-type, maximum detection at 1200 °C) was used to determine the temperature. It is obvious that the observed patterns are identical to the $Bi_4Ti_3O_{12}$ perovskite structure, with the (117)-axis orientation being the most common. Furthermore, there is no indication of secondary phase development in the doped samples. This suggests that the La ions in the $Bi_4Ti_3O_{12}$ perovskite lattice are well dissolved [27].

Low-temperature calcination of coprecipitated precursors was used to directly synthesis rare-earth (RE = La, Nd, Sm) substitution into BiT. The samples were calcined at temperatures ranging from 500 to 800 °C. The XRD intensity of the BiT-based peaks diminishes with increasing RE content at a given temperature, the calcination temperature to generate a well crystalline BiT powder must be elevated with increasing RE content, especially for samples with more than $X = 2.0$ RE substitution and plate-like grains were also observed [22]. Pure Bismuth titanate was prepared by sol-gel method calcined at 500 °C for 14 h. The crystalline nature of BIT begins to emerge at temperatures exceeding 400 °C during annealing. Temperature of maximal thermal treatment (500 °C) There is complete crystallization, monophase formation, and the stoichiometric compound $Bi_4Ti_3O_{12}$ as the predominant crystalline phase. $Bi_4Ti_3O_{12}$ nanoparticles were discovered to have an average crystallite size of 18.82 nm. That's why the formation of agglomerates in BIT appears to be quite large (Fig. 2) [16, 35]. Another method for preparing Bismuth titanate was by conventional solid-state process at a temperature of 700 °C for 48 h. The process was used to make a material with the general formula $Bi_{12+x}TiO_{10+\delta}$ ($0 \le x \le 0.6$) that has a cubic structure with the space group I23 without the trace of any impurity phase [23]. Using a sol–gel technique, a Sm-Ta co-doped $Bi_4Ti_3O_{12}$ ($Bi_{3.96}Sm_{0.04}Ti_{2.92}Ta_{0.08}O_{12}$, BSTTO) thin film was produced on a Pt(111)/Ti/SiO_2/Si(100) substrate and annealed by fast heat annealing (RTA). The BTO thin film contains co-doped Sm and Ta, indicating that the BSTTO thin film is crystallized with the desired (117) orientation. The grains transformed into major platelike and minor rod-like crystals when Sm and Ta ions were present in the BTO thin film. It demonstrates that adding Sm and Ta ions to the BTO thin film changes the grain formation process. With the $(Bi_2O_2)^{2+}$ layers in the ab-plane, the BSTTO thin film may readily achieve a platelike morphology, resulting in a BSTTO thin film with a higher grain size than the BTO thin film [36].

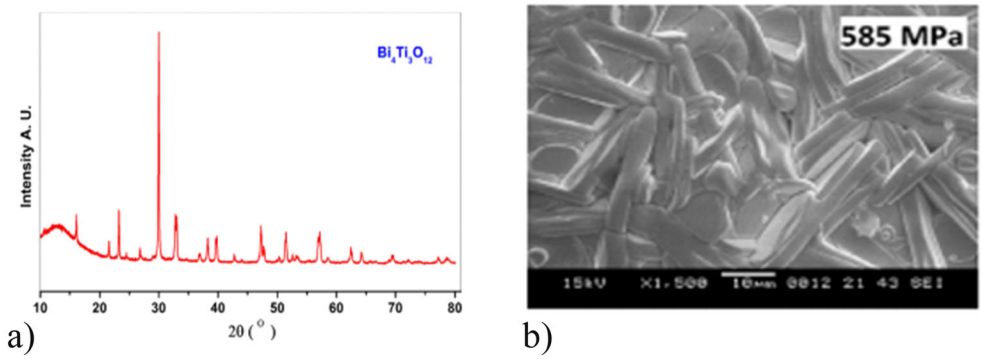

Fig. 2 (**a**) XRD pattern of bismuth titanate (**b**) SEM image of bismuth titanate [35]

3 Ferroelectric properties

$Bi_4Ti_3O_{12}$ is an anisotropic material having a plate-like microstructure, low coercive field, outstanding fatigue properties, minor remnant polarization, a long retention period, etc. The synthesis process has a considerable influence on the structure and properties of $Bi_4Ti_3O_{12}$. The domain structure, the degree of interaction among domain boundaries, and the particular kinds of ferroelectric defects all influence the properties of ferroelectrics. Impedance estimations provide accurate data on defects, domain walls, and any other types of defects. Along these lines, the impedance estimation is found to be a helpful apparatus for concentrating on the defect structure of ferroelectric materials. This investigation not only discloses the defect contribution, yet additionally the relaxation mechanism under a bunch of experimental conditions. The properties of BTO ceramics can be improved by replacement doping of the A-site and B-site with transition metals. It can decrease leakage current and increase ferroelectric properties greatly. BTO ceramics doped with Ce, La, Dy, Pr, Er, Sm, Ta, Nd, and V had previously been examined. Substituting V^{5+} for Ti^{4+} reduces leakage current and enhances ferroelectric characteristics while also improving residual polarization, P_r [15, 17, 33, 36–40]. Dhages et al. prepared $Bi_4Ti_3O_{12}$ using the citrate procedure, demonstrating the effect of preparation on ferroelectric properties in Fig. 3. Estimates of the ferroelectric hysteresis loop properties of the pellet sintered at 1273 K at an applied voltage of 53.6 kV cm^{-1} show values of spontaneous polarization of 9 C cm^{-2}, remnant polarization of 4 C cm^{-2}, and coercive field of 25 kV cm^{-1} without an electric breakdown. The pellet's relative density was 90%. The reported values of these parameters ranged from a coercive field of 25–100 kV cm^{-1} to spontaneous polarization of 24-40 C cm^{-2}, depending on the preparation conditions. The ceramic technique samples exhibit spontaneous polarization, remnant polarization, coercive field as 2 C cm^{-2}, 0.5 C cm^{-2}, and 23 kV cm^{-1} respectively without an electric breakdown at a field of

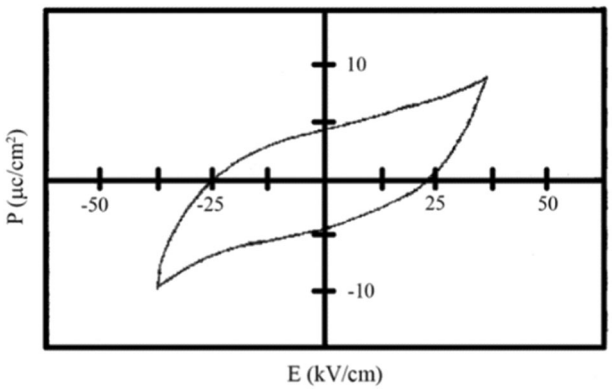

Fig. 3 Shows the hysteresis loop of $Bi_4Ti_3O_{12}$ [41]

Table 2 Remnant polarization (Pr) and coercive field (Ec) for doped and undoped $Bi_4Ti_3O_{12}$ samples

Sample	Remnant polarization	Coercive field	Ref
Pt/SiO_2/Si-doped $Bi_4Ti_3O_{12}$	23.7	3.1	[6]
Pure $Bi_4Ti_3O_{12}$	4	25	[41]
Sm–Ta co-doped $Bi_4Ti_3O_{12}$	46.2	102	[36]
V-doped $Bi_4Ti_3O_{12}$	2.574	22.546	[21]
La-doped $Bi_4Ti_3O_{12}$	9.6	35	[27]

40 kV cm^{-1} [41]. Remnant polarization (Pr) and coercive field (Ec) for doped and undoped $Bi_4Ti_3O_{12}$ samples were given in Table 2. Three overlaying relaxation processes, i.e., three semicircles in the complex impedance diagrams that were very substantially regulated by CNLS fitting, were recognized to bulk, grain boundary, and electrode/interface polarization phenomena in BTO ceramics manufactured by the mixed oxide method. At $T = 200$–500 °C, the activation energies for ac conductivity in polycrystalline $Bi_4Ti_3O_{12}$ ceramics for grain (bulk), grain boundary, and electrode

processes are 0.6 eV, 0.4 eV, and 0.54 eV, respectively. For electrode processes, bulk, grain boundary, and polycrystalline BTO ceramics have the activation energies for relaxation values as 0.46 eV, 0.07 eV, and 0.56 eV respectively. In the case of grain boundaries, the activation energy for relaxation is greater than the activation energy for ac conductivity. But for the electrode process, the results were different as their activation energy for Ac conductivity was found to be higher side than for relaxation. Activation energies for relaxations in a bulk compound are ten times lesser as compared to the activation energy for conductivity [17]. Bismuth titanate includes narrow-angle twin walls for weak-field permittivity of single crystals, and the quantitative clarification of low-frequency dispersions was discovered in these crystals, leading to the following findings as in pseudo-orthorhombic ϵ_a, ϵ_b, and ϵ_e, low-temperature maxima are seen, but the relaxation character comes from a space-charge caused by inhomogeneity in the very high conductivity or at the crystal surface. The frequency dependency could be attributed to domain-wall oscillations if the relaxations arise in b-oriented samples. The fact that the crystals were not poled, that dispersion does not happen where σ is low at lower temperatures, and that dispersion frequencies have no obvious relationship to specimen dimensions suggest that frequency dependence is not of piezoelectric origin [18]. For a high-temperature ultrasound sensor, expanding the terminating temperature prompts an increment in density, but on the other hand, is joined by a decrease in d_{33} values. The thermal stability of BIT with the piezoelectric coefficient was observed. The piezoelectric coefficient of a pressed sample with Oil bath poling is obtained as 17 pC N^{-1} and for thick film, the sample accomplishes the piezoelectric coefficient as 8 pC N^{-1}. Through-thickness ultrasound estimations were carried on aluminum, gentle steel blocks, and the stainless-steel pipe at temperatures equal to 230 °C. For permanent bonding, couplings that are fit for working at a higher temperature will fundamental to have a thermal coefficient of development helpful with every bismuth titanate transducer estimated as 7.9 M K^{-1} [42]. Below T_c, the dielectric loss will be constant and a rapid growth occurs about T_c for all frequencies. Because of charge relaxation and ionic polarization at grain and plate boundaries, the ferroelectric to antiferroelectric transition is more noticeable at lower frequencies. From room temperature to 300 °C, the dielectric constant and dielectric loss are both independent of frequency and temperature; however, above this temperature, the obtained sample shows dispersion in dielectric characteristics. The impedance plot indicates that the Zp value declines with the temperature rise, suggesting the rise in capacitance and reduction in resistance of the material represents an increment in conductivity. Arrhenius plots display the conductivity rises with increasing temperature. The conductivity is observed to be dependent on the mobility of oxygen vacancies in the sample [43]. The component generally relates to bulk properties at higher frequencies, grain boundaries at intermediate frequencies, and the influence of processes happening on electrodes or borders at low frequencies. As an alternative to a centered semicircle on the real axis, the Nyquist plot displays dispersion, indicating a non-Debye kind of relaxation, which could be because of multiple relaxation processes in the material. The enhancement in ferroelectric characteristics with vanadium doping in bismuth titanate ceramic could be due to a decrease in space charge density. Oxygen vacancies formed by certain bismuth vacancies will cluster at domain borders in undoped BTO ceramics, creating significant domain pinning and lowering polarization. The removal of the influence of domain pinning is expected to be possible by reducing bismuth vacancy at A-sites. Another way to produce intrinsic ferroelectricity is to exclude oxygen vacancies created by substituting higher-valent cations for Ti at the perovskite B-site. The replacement of V^{5+} with Ti^{4+} to achieve charge neutrality would be performed by incorporating oxygen into oxygen vacancies. Bismuth and oxygen vacancy complexes are eliminated as a result. As a result, strong domain pinning has less of an impact. Strong domain pinning is reduced to produce large polarization. By reducing domain pinning, vanadium doping in BTO ceramics results in substantially higher polarization than pure BTO ceramics. At ambient temperature, the ferroelectric *P–E* loops for all BVT samples are shown in Fig. 4 at a maximum applied field of roughly 30 kV/cm. With increasing vanadium doping up to 0.024 mol% vanadium, residual polarization (Pr) (1.232–2.482) and coercive field (Ec) (17.244–22.340) for all BVT samples rise. The leakage current is successfully reduced by improving polarization with B-site doping of vanadium into BTO [21].

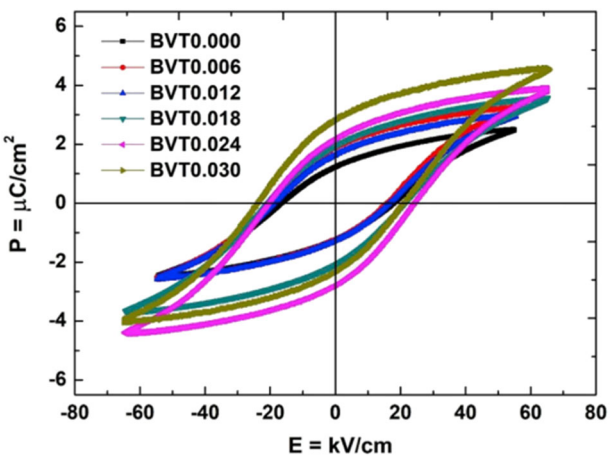

Fig. 4 *P–E* loop for vanadium doped bismuth titanate [21]

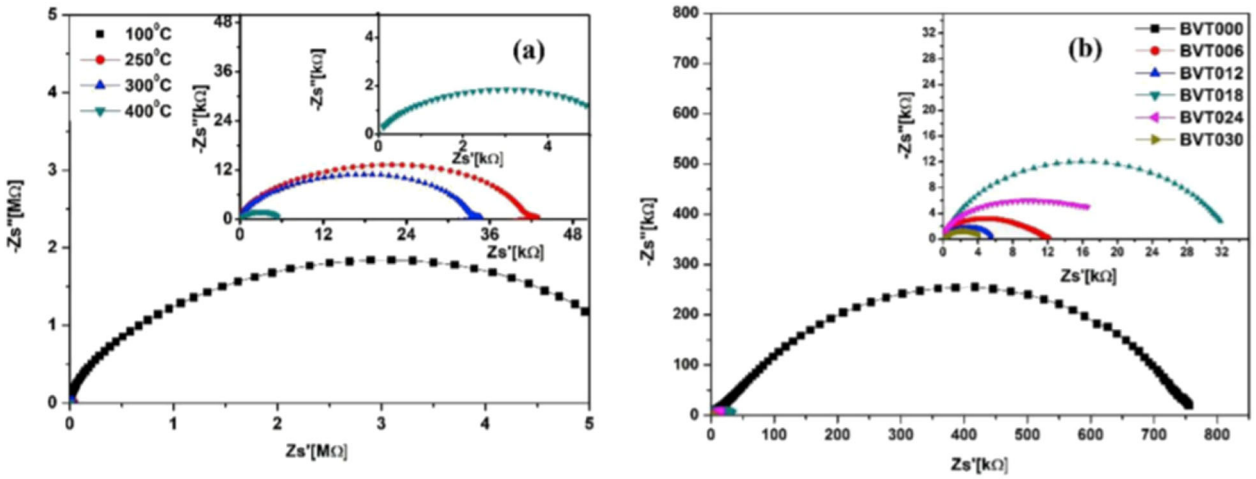

Fig. 5 Nyquist plots for (**a**) 24% of V doped-BTO at various temperatures (**b**) For all V doped BTO at 250 °C [43]

4 Dielectric properties

When a dielectric material is exposed to an exterior electric field, polarization happens, which involves the reverse motion of charges and results in the production of an induced field that is the polar opposite of the applied external field. The dominant contribution to the overall polarization below the microwave frequency range comes from orientation polarization because of induced dipole and permanent dipoles, as well as bilateral and space charge polarization. Losses in the dielectric are connected with the relaxation of various types of polarization. Reduction in polarization occurs once the dielectric is removed from the external electric field, resulting in a return to the equilibrium condition. The Debye model, which predicts relaxation behaviors for identical non-interacting dipoles, does not apply to real dielectrics. Relaxing polarons, quasiparticles related to local lattice deformation generated by moving charge carriers and implicated in the electrical conduction of various materials, attain thermally induced Debye-type relaxation. Relaxation of these sorts of polarization occurs once the dielectric is removed from the external electric field, resulting in the return to the equilibrium condition. Real dielectrics behave differently as compared to the simplistic Debye model, which defines relaxation behaviors for undistinguishable non-interacting dipoles [44]. Hideo Kimura et al. observed the dielectric characteristics of $Bi_4Ti_3O_{12}$ fiber crystals. Dielectric analysis shows that a huge difference of greater than ten times becomes determined for the dielectric constant along the c-axis as compared with the a-axis. From the Arrhenius plot of the inverse impedance and inverse temperature, the activation energies measured above 400 °C were 0.6 eV along the *c*-axis and 0.5 eV along the a-axis. The activation energies for AC conductivity, as well as the c- and a-axes, were measured to be 1.3 and 0.7 eV. So, the conductivity along the *c*-axis is smaller than the a-axis [45]. Below Tc, the dielectric loss is constant and rapidly rises near T_c for all frequencies. The ferroelectric to antiferroelectric transition is more visible at lower frequencies because of charge relaxation and ionic polarization at grain and plate boundaries. From ambient temperature to 300 °C, Frequency and temperature have little effect on dielectric loss and dielectric constant. however, above this temperature, the obtained sample shows dispersion in dielectric characteristics (Fig. 5) [43]. For high-temperature ultrasonic transducers, Elastic modulus, density, permittivity, and conductivity were measured and the d_{33} constant was estimated as 16 Picocoulombs per Newton. This value is greater than that of bulk bismuth titanate, which has been reported. As a result, these films can resist greater field strengths during poling, resulting in higher d_{33} values. [46]. The relative permittivity has a low-frequency dispersion for all temperatures measured due to the presence of conduction processes in the material. Charge carriers must be addressed in the polarization processes in this situation, and relative permittivity has a conductive component ($I\sigma/\omega$) [47]. Rachna et al. studied La-doped $Bi_4Ti_3O_{12}$ ceramics. According to dielectric studies, BLT075 has greater activation energy than BLT0, owing to lower oxygen ion-vacancy concentrations. With the change in the oxygen ion-jump relaxation peak in the temperature dependence of the dissipation factor study, this site-favored replacement became more regular. Because of the decrease in oxygen vacancy concentrations in the perovskite lattice, the temperature dependence of DC conductivity for each of the three contributions revealed that while La-doping did not change the activation energy of plate boundaries, it improved the activation energy of the crystalline layer. It is hypothesized that the Bi-ions were replaced by La-ions rather than the Bi_2O_2 layer [19]. Mukhortov et al. observe the anisotropic dielectric response of $Bi_4Ti_3O_{12}$ films rises with the decline in film thickness along with the crystal

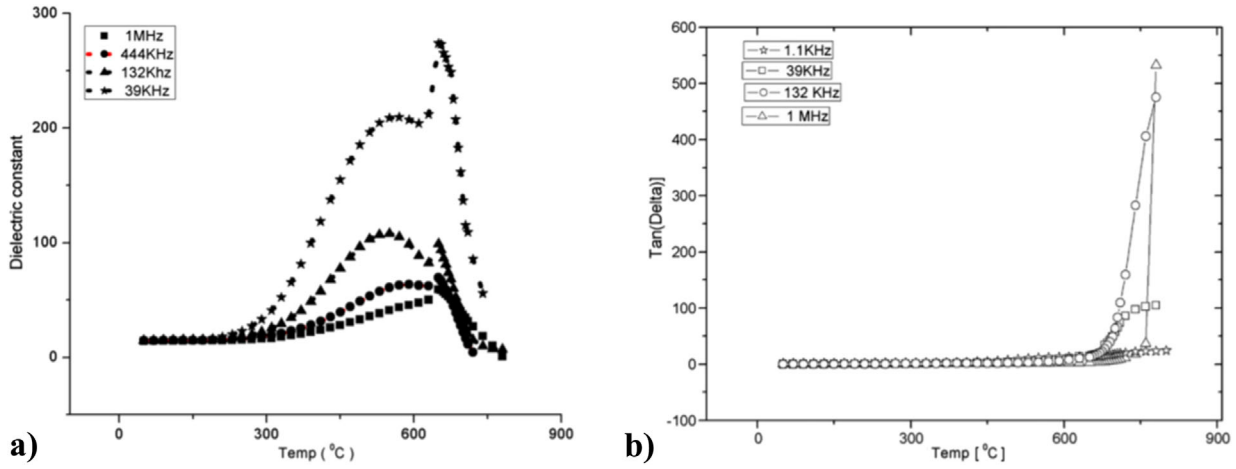

Fig. 6 **a** The dielectric constant varies with temperature at specific frequencies. **b** Dielectric loss at various frequencies as a function of temperature [20]

directions. The dielectric constant in the direction of [100] is higher than in the direction of [110] [48]. The Nyquist plot Fig. 6 displays a non-Debye type relaxation as an alternative to a semicircle, which might be due to the material's numerous relaxation processes arising in the material. The radius of the semicircle reduced as the temperature increased, indicating that it had a lower resistance value at higher temperatures. The radius of the semicircle decreases, suggesting a shorter relaxing time. As the temperature rises, the dielectric constant rises with it. With increasing temperature, charge carrier mobility increases, resulting in increased polarization and a high dielectric constant. Charge accumulation at grain boundaries causes a larger dielectric constant value at high temperatures. The dielectric constant reduces as the frequency rises. At lower frequencies, electronic, ionic, dipolar, and interfacial/space charge polarization all contribute to the dielectric constant; however, beyond 100 kHz, interfacial/space charge polarization's contribution is reduced, resulting in a drop in dielectric constant [16, 34, 35]. The dielectric constant rises as the palletization pressure rise. This is due to the increased density of pellets. The increased dielectric constant reported in these materials can be attributed to the Bi and Ti ions' considerable electronic polarizability in conjunction with their ionic polarizability, as well as the favorable polarization of the internal field [49]. The Dielectric permittivity-temperature curve for the Sm-2.0, La-2.0, and Nd-2.0 and ceramics indicates ε_r is highest (around 540–560 °C) in their curves consisting of anisotropic plate-like grains which corresponded to the ferroelectric–paraelectric phase transition. By increasing the Nd substitution of $X = 2$ to 2.5, structural distortion may be reduced, and the BiT-based phase can become ferroelectric [22, 50, 51]. The dielectric loss (tan δ) of Nd and Sm-doped BiT was observed at 1 MHz that BNdT and BSmT have low tanδ and BNdT have high ε_r [20]. For strongly (117)-oriented BSTTO thin film has a high remanent polarization (2Pr) as 46.2 C/cm^2 and low coercive field ($2E_c$) as 102 kV/cm [36]. The dielectric property of BiT/Ag composites was measured as a function of frequency from 1 kHz to 1 MHz was observed. The dielectric property of BiT/Ag composites was measured as a function of frequency from 1 kHz to 1 MHz. When silver is added to pure BiT ceramic, the dielectric constant increases by up to ten times, owing to the effective electric fields formed around the scattered metal particles as well as the percolation effect. Incorporating silver particles also reduce dielectric losses dramatically, with BiT/Ag composites having dielectric losses of less than 0.5% [24]. The peaks of dielectric constants at Curie temperature grew wider as the composition contained more vanadium. The creation of an extra phase and non-uniform vanadium distribution in the samples might be the source of this phenomenon. According to ferroelectric property measurements, the BTV02 sample's remanent polarization and coercive fields were 12 C/cm^2 and 32.5 kV/cm, respectively. Piezoelectric constants (d33) as large as 20 Picocoulombs per Newton were observed in both BTV02 and BTV04 samples, showing that the addition of vanadium to BIT improves polarization characteristics [52]. Table 3. Shows the dielectric constant and dielectric loss of doped and undoped $Bi_4Ti_3O_{12}$.

5 Applications of bismuth titanate

$Bi_4Ti_3O_{12}$ is a single crystal with a low dielectric permittivity, making it suitable for memory elements, optical displays, and piezoelectric converters in pyroelectric devices across a wide temperature range up to 600 °C [26]. Ceramics made of $Bi_4Ti_3O_{12}$ have been employed in

Table 3 Dielectric constant and dielectric loss of doped and pure bismuth titanate

Sample	Dielectric constant (ε')	Dielectric loss (tanδ)	Ref
Vanadium doped Bi_4 Ti_3O_{12}	403	12.7	[21]
Lanthanum doped $Bi_4Ti_3O_{12}$	354.5	0.874	[34]
Pure $Bi_4Ti_3O_{12}$	450	0.98	[53]

capacitors, transducers, sensors, LTCC multi-layered ceramic technology [21, 35], NvRAM device [30, 52] and other applications. $Bi_4Ti_3O_{12}$ is a ferroelectric material that may be employed in ferroelectric or electrooptic devices in thin film form. $Bi_4Ti_3O_{12}$ is a potential option for ferroelectric random-access memories (FRAM) and dynamic random-access memory due to its high Curie temperature, outstanding fatigue behavior, and tolerable ferroelectric characteristics [34]. $Bi_4Ti_3O_{12}$ films produced on a superconductor shown promising ferroelectric characteristics and the ability to be integrated into semiconductor device processing techniques.

6 Summary and outlook

In summary, the dielectric, and ferroelectric properties of bismuth titanate composites prepared by different methods were reviewed. The domain structure, the degree of contact between domain boundaries, and the different types of ferroelectric defects all have a role in the properties of ferroelectrics. With increasing temperature, charge carrier mobility increases, resulting in increased polarization and a high dielectric constant. Charge accumulation at grain boundaries causes a larger dielectric constant value at high temperatures. The dielectric constant decreases as the frequency rises. At lower frequencies, electronic, ionic, dipolar, and interfacial/space charge polarization all contribute to the dielectric constant; however, at 100 kHz, the contribution from interfacial/space charge polarization decreases, leading to a dielectric constant decrease. Bismuth titanate single-crystal displays spontaneous polarization values of 4 and 50 C/cm^2, coercive field values of 3.5 and 50 kV/cm, and dielectric constant values of 130 and 160, in addition to the c- and a-axes. Activation energies for Ac conductivity were compared to activation energies for grain (bulk), grain boundary, and electrode processes in polycrystalline $Bi_4Ti_3O_{12}$ ceramics. The activation energy for grain boundary relaxation is greater than the activation energy for Ac conductivity. The activation energy for Ac conductivity is larger in the electrode process than in the relaxation process. Similarly, in the case of bulk, the relaxation activation energy is ten times lower than the Ac conductivity.

The disadvantages of BIT include significant dielectric loss, low remanent polarization (Pr), and a large coercive field (Ec). To improve their properties, different types of ions have been doped at the A-sites or B-sites. When vanadium is doped into bismuth titanate, the dielectric constant rises as the vanadium concentration rises, increasing space charge density. The activation energy of plate borders remains unchanged when lanthanum is doped with bismuth titanate, but the activation energy of the crystalline layer is improved due to lower oxygen vacancy concentrations in the perovskite lattice. Because of the effective electric fields created around the scattered metal particles as well as the percolation effect, the dielectric constant of pure BiT ceramic increases by up to ten times when silver is introduced. Adding rare-earth (La, Sm, Nd) with bismuth titanate, the rare earth cations could substitute completely at the Bi sites in $Bi_4Ti_3O_{12}$ up to $x = 2.5$ at 1100 °C. Sm-2.0 ceramics consisting of anisotropic plate-like grains has relative permittivity maxima at 540–560 °C, which matches the ferroelectric–paraelectric phase transition. The depolarization temperature also corresponds to the ferroelectric to antiferroelectric transition as the specimen gets depolarized and loses its piezoelectric activity as the temperature rises. Charge carrier mobility increases as temperature rises, resulting in higher polarization and a high dielectric constant. At high temperatures, charge accumulation at grain boundaries results in a higher dielectric constant value. For Nd- or Sm-substituted Bismuth titanate samples, the spins in the Nd (Sm)-containing sublattices must be slightly tilted or canted in antiparallel alignment. In the case of Lead-free bismuth titanate, Hysteresis measurements show that the remnant polarization and coercive field dependents on an applied electric field. The d_{33} constant for ferroelectric bismuth titanate was found to be 16 pC/N, which is greater than bulk bismuth titanate. Higher the d_{33} value higher the field strength. The ferroelectric to antiferroelectric transition was more visible at lower frequencies. This occurs as a result of charge relaxation and ionic polarization at grain and plate boundaries. In this approach, conductivity in the sample relies on the variety of oxygen vacancies.

Compliance with ethical standards

Conflict of interest The authors declare no competing interests.

Publisher's note Springer Nature remains neutral with regard to jurisdictional claims in published maps and institutional affiliations.

References

1. Pookmanee Pusit, and Phanichphant Sukon (2007) Characterization of bismuth titanate powders. Adv Mater Res 26–28:247–250. https://doi.org/10.4028/0-87849-463-4.247
2. Sun Shujie et al. (2018) Dielectric relaxation and microwave absorption properties of aurivillius-type multiferroic ceramics. Ceram Int 44(8):9942–9949. https://doi.org/10.1016/j.ceramint.2018.03.023
3. Lazarevic Z, Stojanovic B, Varela J (2005) An approach to analyzing synthesis, structure and properties of bismuth titanate ceramics. Sci Sinter 37(3):199–216
4. Noguchi Y, Miwa I, Goshima Y, Miyayama M (2000) Defect control for large remanent polarization in bismuth titanate ferroelectrics—doping effect of higher-valent cations. Jpn J Appl Phys 39(Part 2):12B
5. Simões AZ, Ramirez M, Riccardi C, Ries A, Longo E, and Varela J (2005) Influence of temperature on the dielectric and ferroelectric properties of bismuth titanate thin films obtained by the polymeric precursor method. Mater Chem Phys 92(2–3):373–378
6. Azlan UmarAl-Amani, Ahmad Fauzi Mohd Noor (2017) A study on structural stability of bismuth titanate with lanthanum doping for improved ferroelectric properties. Bull Mater Sci 40 (3):493–498. https://doi.org/10.1007/s12034-017-1387-z
7. Du X, Xu Y, Ma H, Wang J, Li X (2008) Low-temperature synthesis of bismuth titanate by an aqueous sol-gel method. J Am Ceram Soc 91(7):2079–2082
8. Villegas M, Moure C, Fernandez JF, Duran P (1996) Preparation and sintering behaviour of submicronic Bi4Ti3O12 powders. J Mater Sci 31(4):949–955
9. Umabala A, Suresh M, Prasadarao A (2000) Bismuth titanate from coprecipitated stoichiometric hydroxide precursors. Mater Lett 44 (3-4):175–180
10. Aurivillius B (1949) Mixed bismuth oxides with layer lattices. II. Structure of $Bi4Ti_3O_{12}$. Ark Kemi 1(54):463–480
11. Subbarao E (1962) A family of ferroelectric bismuth compounds. J Phys Chem Solids 23(6):665–676
12. Kikuchi T, Watanabe A, Uchida K (1977) A family of mixed-layer type bismuth compounds. Mater Res Bull 12(3):299–304
13. Takenaka T, Sasaki T (1997) New bismuth layer-structured ferroelectrics with niobium ions As B-site. Ferroelectrics 201 (1):117–126
14. Nagata H, Takahashi T, Chikushi N, Takenaka T (2000) A series of bismuth layer-structured ferroelectrics. Ferroelectrics 241 (1):309–316
15. Bernard H, Lisińska-Czekaj A, Dzik J, Osińska K, Czekaj D (2011) Fabrication, structural and AC impedance studies of layer-structured $Bi_4Ti_3O_{12}$ ceramics. Arch Metall Mater 56 (4):1137–1148
16. Gupta P, Balram, and Singh DP, Synthesis and characterization of ferroelectric bismuth titanate (Bi_4Ti3O_{12}). 2014
17. Noguchi Y, Miyayama M (2001) Large remanent polarization of vanadium-doped $Bi_4Ti_3O_{12}$. Appl Phys Lett 78(13):1903–1905
18. Fouskova A, Cross LE (1970) Dielectric properties of bismuth titanate. J Appl Phys 41(7):2834–2838
19. Rachna S, Bhattacharyya S, Gupta S (2010) Correlating structure, dielectric and impedance studies with lanthanum-ion substitution in bismuth titanate. Mater Sci Eng: B 175(3):207–212
20. Thiruramanathan P, Sharma SK, Sankar S, Ganesh RS, Marikani A, Kim DY (2016) Synthesis of bismuth titanate (BTO) nanopowder and fabrication of microstrip rectangular patch antenna. Appl Phys A 122:12
21. Badge SK, Deshpande A (2019) Effect of vanadium doping on structural, dielectric and ferroelectric properties of bismuth titanate ($Bi_4Ti_3O_{12}$) ceramics. Ceram Int 45(12):15307–15313
22. Shigyo Tatsuhiro et al. (2008) Synthesis and dielectric-magnetic properties of rare-earth (La, Nd, Sm)-modified $Bi_4Ti_3O_{12}$. Jpn J Appl Phys 47(9):7617–7622 https://doi.org/10.1143/jjap.47.7617
23. Yuen M, Tan Y, Tan K, Taufiq-Yap Y (2012) Synthesis and characterization of electrical properties of bismuth titanate. Adv Mater Res 501:101–105
24. Xiang P-H, Kinemuchi Y, Watari K (2006) Enhanced dielectric properties of bismuth titanate/silver composites. J Electroceram 17 (2-4):861–865
25. Xia A, Tan G, Ren H (2016) Microwave hydrothermal synthesis of a new bismuth titanate compound. Mater Today Commun 8:134–138
26. Padmanaban A, Dhanasekaran T, Kumar SP, Gnanamoorthy G, Stephen A, Narayanan V (2019) Catalytic activity of bismuth titanate. Mater Today Proc 14:553–557
27. Azlan UAA, Noor AFM, Yusuf Y, Omar N, Mohamad N (2015) Effect of neodymium and samarium on the properties of bismuth titanate ceramics. Appl Mech Mater 761:397–401
28. Axelsson A-K, Alford NM (2006) Bismuth titanates candidates for high permittivity LTCC. J Eur Ceram Soc 26 (10–11):1933–1936
29. Siriprapa P, Watcharapasorn A, Jiansirisomboon S (2009) Electrical and mechanical characteristics of ($Bi_{4-x}La_x$) $Ti3O_{12}$ ceramics. Ferroelectrics 382(1):160–165
30. Badapanda T, Harichandan R, Kumar TB, Mishra SR, Anwar S (2016) Dielecric relaxation and conduction mechanism of dysprosium doped barium bismuth titanate Aurivillius ceramics. J Mater Sci: Mater Electron 28(3):2775–2787
31. Chen M, Liu ZL, Wang Y, Wang CC, Yang XS, Yao KL (2003) Ferroelectric properties and microstructures of Nd_2O_3-doped $Bi4Ti_3O_{12}$ ceramics. Phys Status Solidi (A) 200(2):446–450
32. Dhage S, Khollam Y, Dhespande S, Potdar H, Ravi V (2004) Synthesis of bismuth titanate by citrate method. Mater Res Bull 39 (13):1993–1998
33. Fuentes S, Muñoz P, Llanos J, Vega M, Martin I, Chavez-Angel E (2017) Synthesis and optical characterization of Er-doped bismuth titanate nanoparticles grown by sol–gel hydrothermal method. Ceram Int 43(4):3623–3630
34. Badge SK, Deshpande A (2020) La+3 modified bismuth titanate (BLT) prepared by sol – gel synthesis: Structural, dielectric, impedance and ferroelectric studies. Solid State Ion 347:115270
35. Badge SK, Deshpande A (2018) Effect of pressure of pelletization on dielectric properties of bismuth titanate prepared by sol-gel synthesis. Adv Powder Technol 29(3):555–562
36. Kao M-C, Chen H-Z, Young S-L (2013) The microstructure and ferroelectric properties of Sm and Ta-doped bismuth titanate ferroelectric thin films. Thin Solid Films 529:143–146
37. Subohi O, Singh R, Kumar GS, Malik MM, Kurchania R (2015) Impedance analysis and dielectric properties of Ce modified bismuth titanate lead free ceramics synthesized using solution combustion route. J Mater Sci Mater Electron 26(11):9122–9133
38. Miao F, Tao B, Chu PK (2015) Synthesis, microstructure, and electronic band structure properties of nanocrystalline neodymium-doped bismuth titanate ferroelectric films fabricated by the sol–gel method. Mater Res Bull 61:238–244
39. Bokolia R, Thakur O, Rai VK, Sharma S, Sreenivas K (2015) Dielectric, ferroelectric and photoluminescence properties of Er3 doped Bi_4Ti3O_{12} ferroelectric ceramics. Ceram Int 41 (4):6055–6066
40. Chakraborty P, Krupanidhi SB (2010) Polarization enhancement in compositionally graded vanadium doped bismuth titanate thin films. J Appl Phys 107(12):124105
41. Lazarevic Z, Stojanovic B, Varela J (2005) An approach to analyzing synthesis, structure and properties of bismuth titanate ceramics. Sci Sinter 37(3):199–216

42. Burrows S, Mcaughey K, Edwards R, Dixon S (2012) Sol–gel prepared bismuth titanate for high temperature ultrasound transducers. RSC Adv 2(9):3678
43. Subohi O, Kumar G, Malik M, Kurchania R (2012) Dielectric properties of bismuth titanate (Bi4Ti3O12) synthesized using solution combustion route. Phys B: Condens Matter 407 (18):3813–3817
44. Szwagierczak D, Kulawik J, Witek K (2015) Study on dielectric properties of lanthanum copper tantalate ceramics by impedance spectroscopy. Mater Sci Semiconductor Process 38:329–335
45. Kimura H, Tanahashi R, Maiwa K, Cheng Z, Kannan CV (2007) Crystal growth and electric properties of bismuth titanate fibers. Jpn J Appl Phys 46(10B):7031–7034
46. Searfass CT, Pheil C, Sinding K, Tittmann BR, Baba A, Agrawal DK(2016) Bismuth titanate fabricated by spray-on deposition and microwave sintering for high-temperature ultrasonic transducers. IEEE Trans Ultrason, Ferroelectr, Frequency Control 63(1):139–146
47. Macedo Z, Ferrari C, Hernandes A(2004) Impedance spectroscopy of Bi_4Ti_3O12 ceramic produced by self-propagating high-temperature synthesis technique. J Eur Ceram Soc 24(9):2567–2574
48. Mukhortov VM, Golovko YI, Anokhin AS, Stryukov DV, Biryukov SV, Timoshenko PE (2019) Structure, lattice dynamics, properties of bismuth titanate heterostructures. J Phys D: Appl Phys 53(3):035304
49. Stanislav SSlavov, Milena ZKrapchanska, Elena PKashchieva, Svetlin B, Parvanov, Yanko BDimitriev(2012) Dielectric properties of bismuth titanate 354 ceramics containing SiO_2 and Nd_2O3 as additives. Process Appl Ceram 6(3):117–122 353
50. Yau CY, Palan R, Tran K, Buchanan RC (2005) Mechanism of polarization enhancement in La-doped $Bi_4Ti_3O_{12}$ films. Appl Phys Lett 86(3):032907
51. Srinivas A, Kim D-W, Hong KS, Suryanarayana S (2004) Study of magnetic and magnetoelectric measurements in bismuth iron titanate ceramic—$Bi8Fe_4Ti3O_{24}$. Mater Res Bull 39(1):55–61
52. Tang Q-Y, Kan Y-M, Li Y-G, Zhang G-J, Wang P-L (2006) Effect of vanadium doping on fabrication and property of Bi_4Ti3O_{12} ceramics. Scr Mater 54(12):2075–2080
53. Lin X, Lv P, Guan Q, Li H, Zhai H, Liu C (2012) Bismuth titanate microspheres: directed synthesis and their visible light photocatalytic activity. Appl Surf Sci 258(18):7146–7153